Mon. Not. R. Astron. Soc. **399,** 1145–1156 (2009) doi:10.1111/j.1365-2966.2009.15365.x

Origin and structure of the Galactic disc(s)

Ralph Schönrich[1,2⋆] and James Binney[3]

[1]*Max-Planck-Institut für Astrophysik, Karl-Schwarzschild-Str. 1, D-85741 Garching, D*
[2]*Universitätssternwarte München, Scheinerstr. 1, D-81679 München, D*
[3]*Rudolf Peierls Centre for Theoretical Physics, Keble Road, Oxford OX1 3NP*

Accepted 2009 July 3. Received 2009 June 27; in original form 2009 February 19

ABSTRACT

We examine the chemical and dynamical structure in the solar neighbourhood of a model Galaxy that is the endpoint of a simulation of the chemical evolution of the Milky Way in the presence of radial mixing of stars and gas. Although the simulation's star formation rate declines monotonically from its unique peak and no merger or tidal event ever takes place, the model replicates all known properties of a thick disc, as well as matching special features of the local stellar population such as a metal-poor extension of the thin disc that has high rotational velocity. We divide the disc by chemistry and relate this dissection to observationally more convenient kinematic selection criteria. We conclude that the observed chemistry of the Galactic disc does not provide convincing evidence for a violent origin of the thick disc, as has been widely claimed.

Key words: Galaxy: disc – solar neighbourhood – galaxies: abundances – galaxies: evolution – galaxies: ISM – galaxies: kinematics and dynamics.

1 INTRODUCTION

Our Galaxy's stellar disc was first divided into two components because the vertical density profile derived from star counts could be fitted by a superposition of two exponentials but not by a single exponential (Gilmore & Reid 1983). Further investigations revealed a thick-disc component that was characterized by a high-velocity dispersion, high α enrichment and a remarkably old age. Many authors consider the thick disc to be a relic of a turbulent era of Galactic history in which the thick disc formed from accreted satellites and/or a thin disc was violently heated by one or more merger events (for a discussion, see e.g. Reddy, Lambert & Allende Prieto 2006). A violent origin of the thick disc is strongly supported by traditional models of chemical evolution (see e.g. Chiappini, Matteucci & Gratton 1997). These models require a period of rapid star formation early in the life of the disc, followed by a period in which star formation effectively ceased in which the interstellar medium (ISM) could be enriched with iron by Type Ia supernovae (SNeIa) and the overall metallicity level could be brought down by accretion of metal-poor gas.

In an earlier paper (Schönrich & Binney 2009, hereafter SB09), we showed that when one allows for radial mixing, which is an unavoidable consequence of spiral structure (Sellwood & Binney 2002; Roskar et al. 2008), a two-component disc arises naturally in the simplest model, in which the star formation rate (SFR) is a monotonically declining function of time from its global maximum. In this paper, we examine in greater depth the contents of the model's solar neighbourhood, especially its characteristic stellar populations. We identify the solar-neighbourhood signatures of the thin and thick discs, and analyse the relationship between the chemistry and kinematics of nearby stars. This exercise enables one to understand better the relationship between the underlying nature of the thin and thick discs and samples of stars that have been selected by kinematic, chemical or spatial criteria. A better understanding of this relationship is of considerable practical importance because substantial allocations of telescope time are currently committed to spectroscopic surveys (SEGUE, RAVE, HERMES, WFMOS, *Gaia*) that are designed to unravel the nature and history of the thick disc, and a clear picture will not emerge from these surveys without a secure understanding of selection effects.

The paper is structured as follows. In Section 2, we summarize the physics that underlie the model and analyse its prediction for the disposition of solar-neighbourhood stars in the ([Fe/H], [α/Fe]) plane. We identify the thin and thick discs within this plane, and show how the kinematics and ages of stars vary within the ([Fe/H], [α/Fe]) plane. The structures we identify seem to have all the properties expected of the Galaxy's thin and thick discs. In Section 3, we explore the extent to which stars can be successfully assigned to the thin and thick discs by kinematic selection. We show that this process cannot be clean. Finally, in Section 4 we sum up and relate the characteristics of the features we have identified to the formation history of our model. Since the SFR in the model has been monotonically decreasing from its global maximum, and no merger or tidal event has ever occurred in it, we conclude that, contrary to widespread belief, features of the Galaxy, such as the

⋆E-mail: rasch@mpa-garching.mpg.de

overlap in [Fe/H] of the thin and thick discs, do not in fact constitute convincing evidence for a violent origin of the thick disc.

2 THE MODEL

2.1 Physical inputs

The SB09 model is the endpoint of a simulation of chemical evolution within a disc in which the SFR, which is controlled by the surface density of the ISM as in the Kennicutt (1998) law, declines monotonically with time from a unique global maximum. The gas disc always has an exponential surface density with scalelength 3.5 kpc so that by the Kennicutt law the young stellar disc has an exponential surface density with scalelength 2.5 kpc. The assumptions regarding the (universal) initial mass function, stellar lifetimes and yields are also taken from the literature. The only novel features are a radial flow of gas within the disc and radial migration of stars. The latter occurs both because over time stars change their angular momenta (churning) and because they move on orbits that become increasingly eccentric and inclined to the Galactic plane (blurring). Traditional models of Galactic evolution have ignored these effects although it has always been evident that blurring occurs. The importance of churning was only realized when Sellwood & Binney (2002) found that even weak spiral structure in N-body simulations causes stars to shift their guiding centres by a kiloparsec and more in a single dynamical time. These motions, which arise when a star is at the corotation resonance with a spiral arm, do not heat the disc, so they come to light only when the angular momenta of individual stars are followed. In the model, the extent of churning is governed by a parameter $k_{\rm ch}$ that could be determined from N-body models if we knew the past strength of spiral structure. SB09 determined $k_{\rm ch}$ by fitting the model to the distribution of solar-neighbourhood stars in [Fe/H]. The radial dependence of churning strength was taken to be proportional to the product of surface density and radius $\Sigma\, R$, following an argument based on disc instabilities.

The dashed green line in Fig. 1 shows the distribution of birth radii of stars in the model Geneva–Copenhagen survey (GCS) sample. Because the GCS stars lie near the plane, the fraction of these stars that are young is higher than the fraction of young stars in the entire solar cylinder. This bias towards young stars leads to the distribution of birth radii of GCS stars being narrower than the distribution of birth radii for all stars in the solar cylinder, which is shown by the full red curve in Fig. 1. The difference between the two distributions is largest for stars born at $\lesssim$5 kpc because those inner disc stars have larger vertical velocity dispersions and therefore larger scaleheights.

Hot gas was assumed to be too far from the disc to take part in churning, while the cold gas and stars were assumed to be equally involved in this process. It is likely that these assumptions exaggerate the impact of churning on old stellar populations, which have high-velocity dispersions, relative to its impact on young stellar populations. Since there is as yet no basis for quantifying the impact of velocity dispersion on churning rate, the model of Paper I avoids additional undetermined parameters by ignoring this possibility.

The flow of gas within the disc enables the surface density of star formation to be an exponential function of radius even though the rate at which accreted gas joins the disc does not necessarily vary exponentially with radius. The surface density of inflow of metal-poor gas and the flow of gas within the disc are jointly controlled by two parameters, $f_{\rm A}$ and $f_{\rm B}$, which substitute for a knowledge of the radial profile of cosmic infall. Attempts to obtain the latter from simulations (e.g. Colavitti, Matteucci & Murante 2008) have not been successful, probably because much of the gas that joins the disc spends a significant time after infall in the warm–hot intergalactic medium. Hence, at the present time we must parametrize the infall in some way. SB09 found that $f_{\rm B}$ is effectively set by the measured oxygen gradient in the ISM, and $f_{\rm A}$ was fitted alongside $k_{\rm ch}$ to the local metallicity distribution of stars. Fig. 2 shows the fit that was obtained to data for $\sim$10 000 non-binary stars in the Geneva–Copenhagen survey (Nordström et al. 2004; Holmberg, Nordström & Andersen 2007).

The random velocities of stars formed at a given radius are assumed to increase with age τ as $\tau^{1/3}$ in line with the predictions of both theory (Jenkins 1992) and studies of the solar neighbourhood (Just & Jahreiss 2007; Aumer & Binney 2009). We have modified the SB09 model very slightly by increasing the $\langle v_R^2\rangle^{1/2}$ of a 10 Gyr old population of local stars from 38 km s^{-1} (cf. Dehnen & Binney 1998) to 45 km s^{-1}. This increase brings the $\langle v_R^2\rangle^{1/2}$ for the entire GCS sample into line with the observed value. In concordance with observations (e.g. Lewis & Freeman 1989), the square of the intrinsic velocity dispersion at a given age is assumed to scale with radius as $\mathrm{e}^{-R/1.5R_*}$, where $R_* = 2.5$ kpc is the scalelength of the stellar disc, so $\langle v_R^2\rangle^{1/2} \simeq 90$ km s^{-1} at $R = R_*$. The square of the vertical

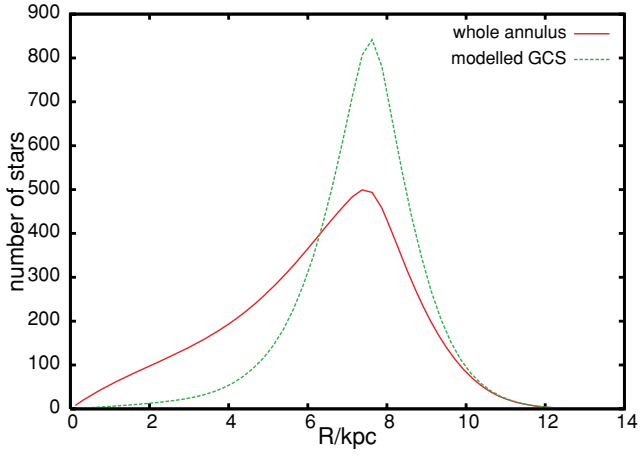

Figure 1. The distribution of birth radii of stars in the model GCS sample (green dashed line) and of all stars in the solar cylinder (solid red line).

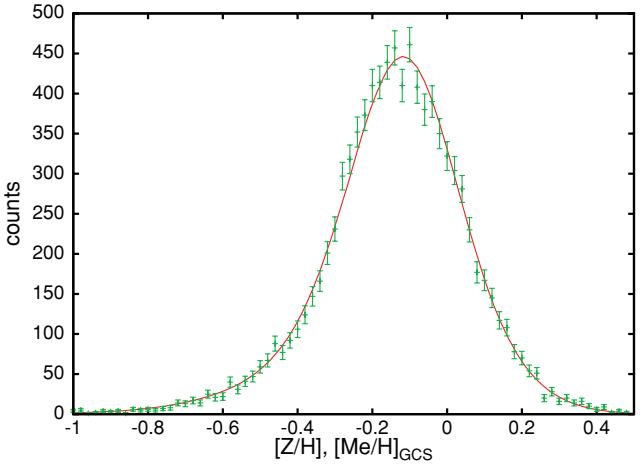

Figure 2. The metallicity distribution of solar-neighbourhood stars: data points from Holmberg et al. (2007); red curve the SB09 model. For the model, total metal abundance is plotted horizontally, while for the data the plotted quantity is the photometric metallicity indicator given in Holmberg et al. (2007).

velocity dispersion component is assumed to show a slightly steeper rise (implying approximately constant scaleheight) being proportional to e^{-R/R_*}.

2.2 Predictions of the model

The merit of the SB09 model is that it tracks the kinematics of stars in addition to their chemistry. Observations always have a kinematic bias of some kind, either because they are restricted to stars that lie near the Sun and therefore the plane, a region favoured by stars with small vertical velocity dispersions, or (as in Juric et al. 2008; Ivezic et al. 2008) because they focus on faint stars that are far from the plane, or because an explicit high-velocity criterion is applied in order to reduce contamination of a thick-disc sample by thin-disc stars. A model that includes both chemistry and kinematics is essential for the interpretation of a kinematically selected study.

The SB09 model makes predictions for the global structure of the Galaxy's stellar and gas discs, but in this paper we focus on the solar neighbourhood, and especially the stars that happen to lie within 100 pc of the Sun. This volume is of particular interest because within it G-dwarfs are bright enough to have good *Hipparcos* parallaxes, measured radial velocities and in a few cases medium-to-high-resolution spectra from which detailed chemical abundance patterns can be extracted. The GCS provides space velocities, surface gravities and metallicities for this volume, and detailed abundance analyses have been carried out for much smaller subsets of stars (Fuhrmann 1998; Bensby, Feltzing & Lundström 2003; Venn et al. 2004; Bensby et al. 2005; Gilli et al. 2006; Reddy et al. 2006). Because the GCS sample is essentially magnitude limited, it is not representative of the volume typically simulated by models of chemical evolution, namely a cylindrical annulus around the disc. In particular, thick-disc stars are underrepresented within the GCS relative to a cylindrical annulus. The SB09 model provides an arena in which the impact of this bias can be assessed.

Fig. 3 shows the densities of simulated GCS stars in the ([Fe/H], [Ca/Fe]) (upper panel) and ([Fe/H], [O/Fe]) (lower panel) planes. Trajectories of the cold ISM at galactocentric radii of 10, 7.5, 5, 2.5 kpc (from left to right) are indicated by black lines. The ISM starts at early times with low-metallicity and high α enhancement at the top left of each panel. As the gas is enriched with metals, each trajectory moves to the right. With the onset of SNeIa, the composition of stellar yields shifts towards iron, so [α/Fe] decreases and the trajectories move downwards. Eventually, the ISM approaches a steady state in which additional enrichment is balanced by the infall of fresh metal-poor material from the intergalactic medium. Since the delay of SNIa enrichment is assumed to be independent of environment, the time at which trajectories first move downwards is independent of radius. By the fact that the time-scale of SNIa enrichment does not vary with radius either, the ISM trajectories tend to be nearly aligned. Thus, the point of turndown is at higher metallicities (further to the right) for populations closer to the Galactic Centre, where the ISM is enriched faster by more intense star formation relative to the present gas mass.

The colours and green contours in Fig. 3 show the density of stars within each plane. In each panel, two ridges of high density are apparent – one at high [α/Fe], which we call the metal-poor thick disc, and one at low [α/Fe], which is associated with the thin disc. Crucially, the thin-disc ridge runs at a large angle to the black trajectories of the ISM. Thus, the thin-disc ridge in no sense traces the chemical history of the thin disc; instead, it reflects the spread in radii of birth of local stars, which gives rise to a spread in [Fe/H] by virtue of the metallicity gradient within the ISM (which is larger in the SB09 model than in traditional models of chemical evolution). In a similar manner, the thick-disk ridge follows the evolution of all rings at low metallicities, but stretches significantly to higher [Fe/H] than the point at which the solar annulus leaves it.

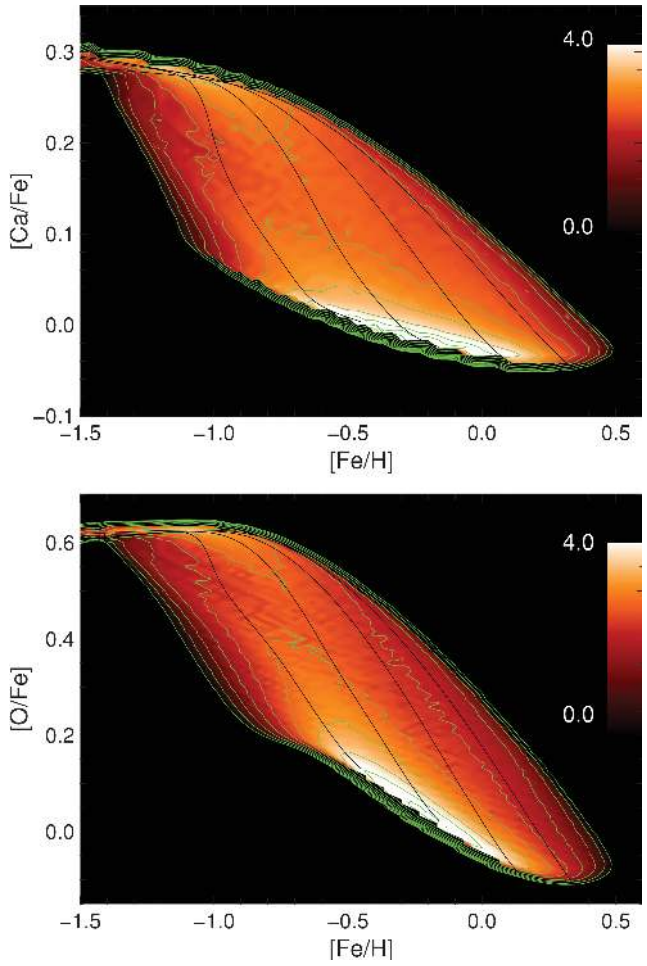

Figure 3. Logarithmic stellar densities for a simulated GCS stellar sample in the ([Ca/Fe], [Fe/H]) (top panel) and ([O/Fe], [Fe/H]) (bottom panel) planes. Contours have a 0.5 dex spacing. Black lines track the development of the cold ISM in annuli of radii of (from right to left) 2.5, 5.0, 7.5 and 10 kpc.

The depression in the stellar density between the ridges in Fig. 3 is a consequence of the rapid downward motion of all trajectories after the onset of SNeIa and of the ISM approaching a steady state as it enters the thin-disc ridgeline; relatively few stars are formed at intermediate values of [α/Fe]. Variations in the time-scales of enrichment will change the depth of the depression – for example, a shorter time-scale for the decay of SNIa progenitors will cause trajectories to move downwards faster, leading to fewer stars in the intermediate region. Our models use a prescription for SNeIa that is standard for models of chemical evolution, with no SNIa until 0.15 Gyr after star formation, and then an exponential decay in the rate of SNeIa with time constant 1.5 Gyr. Mannucci, Della Valle & Panagia (2006) suggest that approximately half of SNeIa explode promptly (within 0.1 Gyr of star formation) and the rest explode at a rate that declines exponentially with time constant 3 Gyr. The existence of prompt SNIa would not materially affect our work as long as a significant fraction of SNeIa are in the population with a long time constant, since the prompt SNeIa

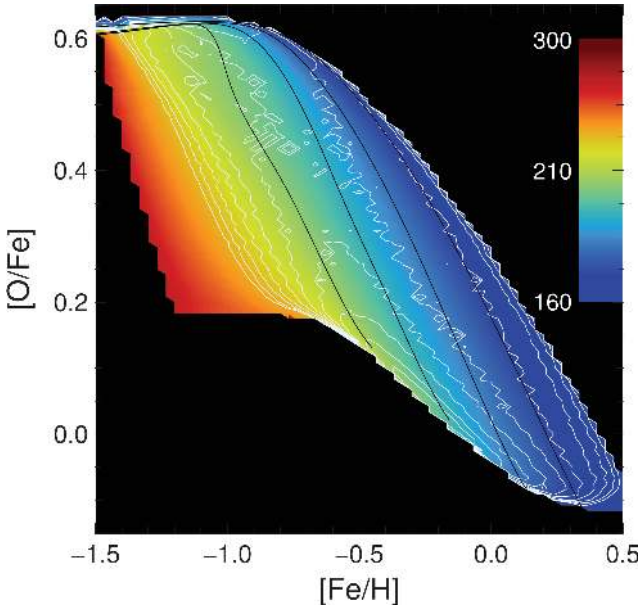

Figure 4. The structure of a simulated sample of GCS stars in the ([Fe/H], [O/Fe]) plane. Contours spaced by 1 dex give the density of stars in this plane, while colour codes the average rotational velocity of the stars found at the point in question – the local circular speed is assumed to be 220 km s^{-1}. Black lines give the trajectories of the cold ISM during the model Galaxy's evolution for galactocentric distances of (from left to right) 10, 7.5, 5, 2.5 kpc.

will lower the α-enhancement level of the thick-disc component but not affect the evolution between the two density ridges in the abundance plane. Förster et al. (2006) showed that time-scales are very weakly constrained by SNIa counts due to uncertainties in the star formation histories.

Since both Ca and O are α-elements, the distributions in the upper and lower panels of Fig. 3 are qualitatively similar, and O will be the only α-element explicitly discussed below.

As Haywood (2008) has pointed out, the principal tracers of radial mixing are the large dispersion in the metallicities of stars in the solar neighbourhood and the strong increase in this dispersion with age, which is caused by immigration of high-metallicity stars from inwards and low-metallicity stars from outwards. In fact, as SB09 demonstrated, it is impossible to fit the shape of the local metallicity distribution under plausible assumptions without radial mixing.

As well as generating a large dispersion in the metallicities of old stars, radial migration has a big impact on the interdependence of kinematics and chemistry. This impact is illustrated by Fig. 4, which is another plot of the ([Fe/H], [O/Fe]) plane, but now with colour indicating the mean rotation velocity of stars at each point – blue indicates low rotation velocities and red large ones. We see that at any given value of [α/Fe], there is a tight correlation between [Fe/H] and rotation velocity in the sense that high [Fe/H] implies low rotation velocity because stars with high [Fe/H] are migrants from small radii and tend to be deficient in angular momentum, while stars with low [Fe/H] are migrants from large radii. The black lines that show the trajectories of the ISM almost constitute contours of constant mean rotation velocity, but there is a barely perceptible tendency for the rotation velocity to decrease as one moves up along a black line.

While the correlation between [Fe/H] and rotation velocity seen in Fig. 4 is qualitative consistent with stars being scattered to more eccentric orbits while retaining their angular momenta (blurring), quantitatively changes in angular momentum (churning) play a big role in structuring Fig. 4. While churning does occasionally move the guiding centre radius of a star from $R_g < R_0$ to $R_g > R_0$ and thus increase the mean rotation speed at large [Fe/H], the dominant effect of churning is to move guiding centres from $R_g \ll R_0$ to $R_g < R_0$ such that a *very* metal-rich star is found in the solar neighbourhood at a relatively low rotation velocity. To illustrate the impact of churning quantitatively, if angular momentum were conserved, the population born 5 kpc from the Galactic Centre would have $v_\phi \sim 150$ km s^{-1}, while stars born at 10 kpc would have $v_\phi \sim 300$ km s^{-1}. In the simulated sample, the mean speeds associated with these radii of birth are actually 200 and 240 km s^{-1}.

Churning substantially increases the chemical heterogeneity of the stars that one finds near the Sun with a given velocity V: if high-α, high-[Fe/H] stars were brought to the Sun only by blurring then all stars with a given V and therefore angular momentum would have identical chemistry. By changing the angular momenta of stars, churning ensures that stars of a given chemical composition are seen near the Sun over the whole range in V.

In Fig. 4, the density of stars is indicated by white contours, which are spaced by 0.5 dex. The very top edge of the populated region is shaded blue, indicating low rotation velocities. Thus, the highest α stars form a structure with a large asymmetric drift. This fact reflects the large velocity dispersion of these stars and the increased opportunity for migration enjoyed by this old population. Note that in this region of the diagram the colour rapidly changes to red as one moves downwards. Hence, there is also a population of high-α stars that have large rotation velocities. These are typically slightly less old stars that formed outside the solar radius. The thin-disc ridgeline at low α enhancement ranges from the strongly trailing at high metallicities to high rotational velocities and slight α enhancement at low [Fe/H], as found observationally by Haywood (2008).

In Fig. 5, the contours show stellar density in increments of 0.5 dex and colours encode the mean age of stars, with blue implying youth. Naturally, the oldest stars are high up, in the region of high [α/Fe]. Right at the top, lines of constant age run almost

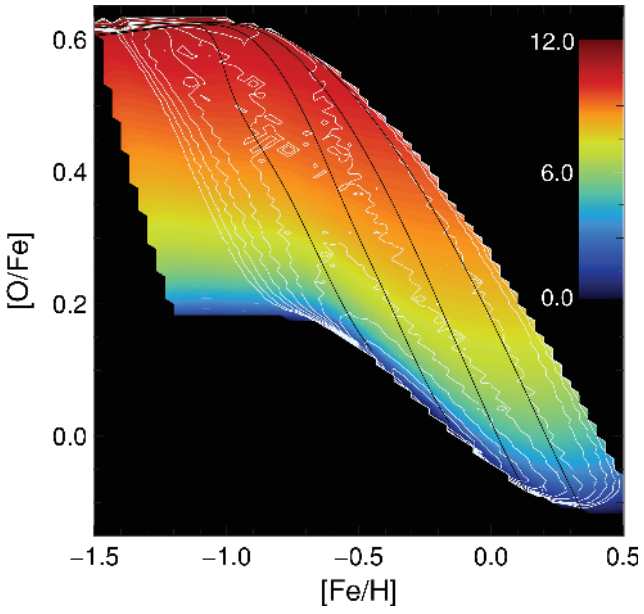

Figure 5. Same as Fig. 4 with colour coding for age and 0.5 dex spacing for density contours.

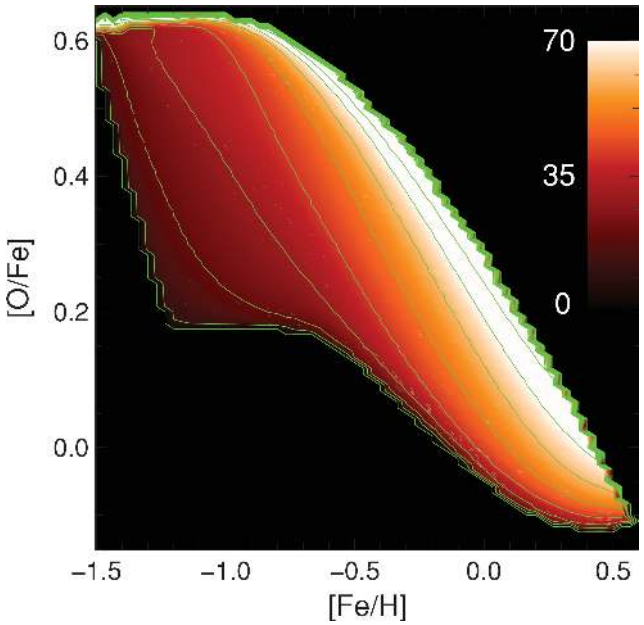

Figure 6. Velocity dispersions (in $\mathrm{km\,s^{-1}}$) as functions of position in the ([Fe/H], [O/Fe]) plane. The graph is derived for a solar-neighbourhood sample by measuring the velocity dispersions of the populations with a specific chemical fingerprint. Two effects act on the velocity dispersion: the dependence on age mostly induces a top-down gradient following the evolution lines of the ISM. In the perpendicular direction (left to right), velocity dispersion increases with decreasing galactocentric radius. The low dispersion of the Galactic thin disc is visible on the lower-left side, girded by a high-dispersion band running from top left to bottom right.

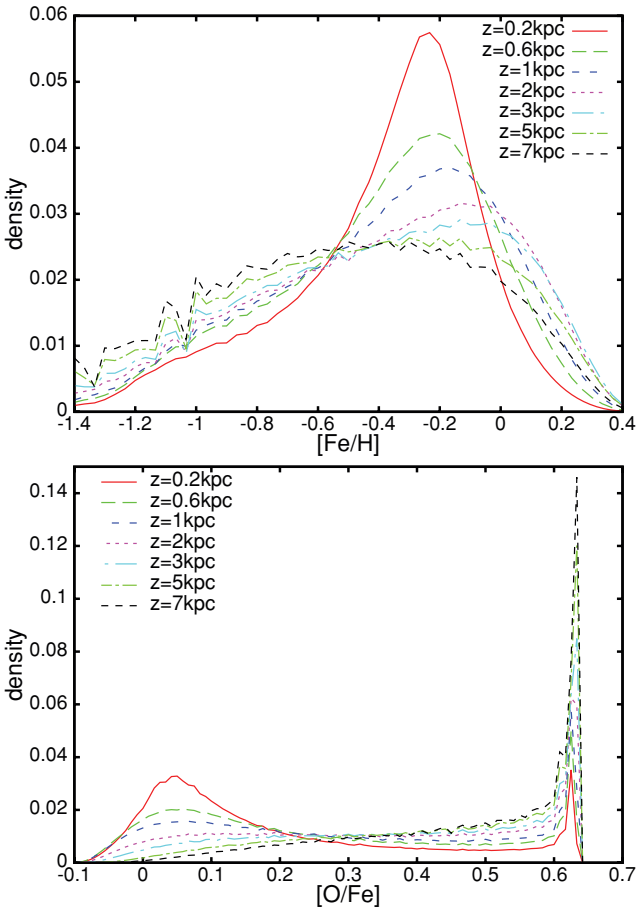

Figure 7. The model's stellar metallicity distributions at different heights above the plane at R_0. Here, we avoided implying a specific selection function by using the mass of a specific population to determine its weight in the distribution. The diagrams are unsmoothed and the scatter comes from the radial (0.25 kpc) and temporal (30 Myr) resolution of the model. Upper panel: distributions of iron abundance. Lower panel: distributions of relative oxygen abundances.

horizontally. As one descends the diagram, lines of constant age slope more steeply down to the right as a result of the more rapid decline in [α/Fe] at small radii. The youngest stars both from outer and from inner rings have yet to reach the solar neighbourhood in significant numbers, so in Fig. 5 several white contours are crossed as one moves along the thin-disc ridge from the location of the solar-radius ISM.

In Fig. 6, both colours and contours (10 $\mathrm{km\,s^{-1}}$ spacing) show the velocity dispersion σ_U of stars of a given chemical composition. The structure of the figure is the product of two mechanisms. (i) The velocity dispersion of stars born at any given radius scales with the third power of age, so older stars have larger velocity dispersions than younger stars born at the same locations. Consequently, in the figure velocity dispersion tends to increase from bottom to top. (ii) Velocity dispersion increases inwards, so stars that have reached the solar neighbourhood from small radii of birth have larger velocity dispersions than stars that have reached us from large radii. When this fact is combined with the fact that for any given date of birth more metal-rich stars are born at smaller radii, a steep rise in σ_U from left to right arises in Fig. 6. This plot suggests that we should include the region of high-velocity dispersion along the upper-right part of the populated region in the thick disc.

Since the single populations have – according to their ages and places of birth – different vertical dispersions, the older populations and those coming from inner radii will have higher scaleheights and so reduced weights in a local sample. However, these populations dominate the composition high above the Galactic plane. The upper panel of Fig. 7 depicts the iron abundance distributions of the stars at different heights above the plane. Both tails of the distribution are strengthened as one moves away from the plane. The growth in the proportion of metal-rich stars with $|z|$ is at first unexpected, but is a natural consequence of the higher vertical velocity dispersion of stars in the inner disc. Notwithstanding the growth of the metal-rich wing of the metallicity distribution, the mean metallicity falls with increasing $|z|$ by more than 0.2 dex, while the dispersion increases from below 0.3 to 0.5 dex. We expect the model, however, to underestimate the vertical metallicity gradient on account of our assumption that a star inherits the velocity dispersion of the galactocentric radius at which it was born. A better model would take account of the actual migration paths of stars – how long each star spent with its guiding centre at each radius. It would predict smaller scaleheights for populations of stars born in the inner disc. Thus, the model might predict too high a fraction of high-metallicity stars to high altitudes.

The metallicity distribution at high altitudes depends on the weakly constrained early evolution of the disc and on details of mixing, so comparisons with observational data would provide valuable constraints on these less secure aspects of the model. Unfortunately, such comparisons are not feasible at present. In particular, we cannot compare with the Sloan Digital Sky Survey (SDSS) data of Ivezic et al. (2008) because their metallicity determination breaks down above [Fe/H] ~ -0.5 dex. The model, however, has a

constant mean rotational velocity in the metallicity range probed by the SDSS survey, in line with the data of Ivezic et al. (2008).

The lower panel of Fig. 7 shows the [O/Fe] distributions at different heights. It reveals the bimodal structure that motivates the division of the disc into two. The exact shape of the two peaks as well as the number of stars in between depend on assumptions about gas enrichment and the behaviour of SNeIa, but the bimodality of the distribution is a fundamental prediction of the model, as was shown in the appendix of SB09. The increasing bias to high ages as $|z|$ increases is reflected in the growing strength of the high [O/Fe] peak relative to the low [O/Fe] peak associated with the thin disc.

2.3 The disc divided

There are principally two strategies by which the disc has classically been dissected by kinematics and by chemistry. We caution that different selection procedures do yield intrinsically different samples and that in general these are not equivalent. We will see that these selection differences, which account for the spread by almost an order of magnitude in estimates of the relative local densities of the thick and thin discs, are readily understood in the context of our model. In each scheme, criteria are set that define both thin- and thick-disc components, while stars that meet neither criterion are here assigned to an 'intermediate population'. We turn first to chemical selection and then in the light of this assess the quality and effects of kinematical criteria.

The dots and crosses in the upper panel of Fig. 8 show a realization of a GCS-like sample of stars in the model. The ridge of the thin disc is evident, as is a ridge of metal-poor thick-disc stars at [Fe/H] $\lesssim -0.65$ and [O/Fe] ~ 0.6. We consider the thin disc to consist of all stars that lie within the black lines around this ridge. Less clear is the extent of the thick disc at [Fe/H] $\gtrsim -0.6$. Guidance is provided by plotting in green the locations of those stars in the realization that satisfy the kinematic selection criteria of Bensby et al. (2003) to belong to the thick disc. A few of these stars lie in the region reserved for the thin disc; this phenomenon illustrates the inability of any kinematic selection criteria to separate cleanly the thin and thick discs (see Section 3). In light of the distribution of green crosses in Fig. 8, we define the thick disc to consist of all stars that lie either above the horizontal line at [O/Fe] $= 0.56$ or to the right of the sloping line, which has the equation

$$[\mathrm{O/Fe}] = 0.56 - 0.55([\mathrm{Fe/H}] + 0.8). \quad (1)$$

The lower panel of Fig. 8 shows the chemical compositions of stars in three large observational programmes. These studies used different selection criteria – Bensby et al. (2005) kinematically selected for thick-disc stars, while Gilli et al. (2006) studied stars with planets, so their stars are all metal-rich.

The top and centre panels of Fig. 9 show the distributions of rotation velocity (top panel) and age (centre panel) within the thin disc (green), the thick disc (red) and the intermediate population (blue) when the local stellar population is divided in this way. In the top panel, the thick disc stands out for the extent to which its V-distribution extends to low V. However, its peak lags circular rotation by only $\sim$10 km s^{-1} because it has a significant extension to $V > 0$. On account of its long tail, the average asymmetric drift of the thick disc is $\sim$22.5 km s^{-1}, which is slower than that of the thin disc by $\sim$18 km s^{-1}. The intermediate population is much more symmetrically distributed in V and, like the V-distribution of the thin disc, peaks near $V = 0$ with an average drift of $\sim$10 km s^{-1}. Note that these velocities are relative to the local standard of rest (LSR), rather than the Sun, which is rotating faster than the LSR by

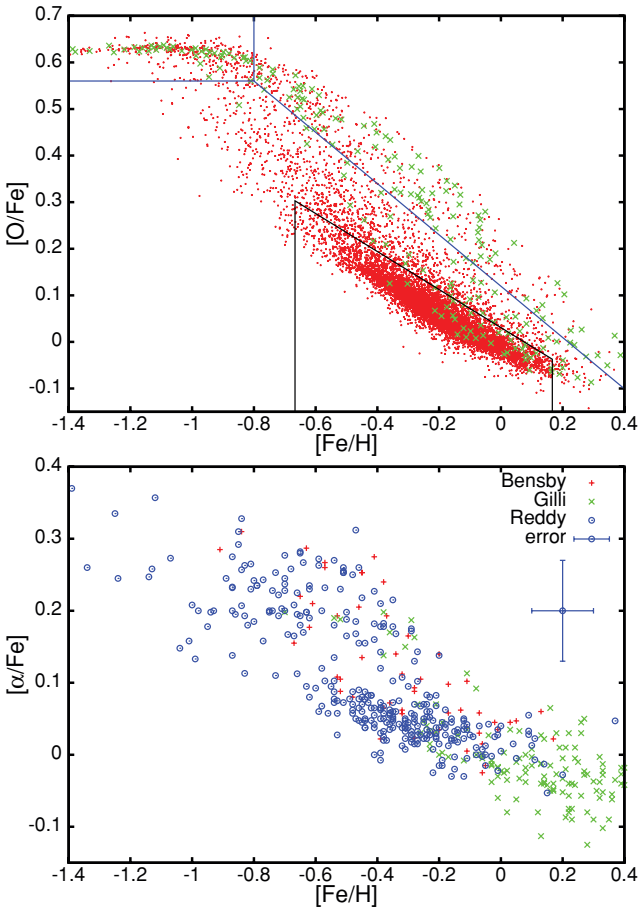

Figure 8. Upper panel: a scatter plot for a GCS-like measurement of solar-neighbourhood stars in the ([Fe/H], [O/Fe]) plane. Red dots mark positions of stars, while green crosses mark stars that are selected to the thick disc via the kinematic selection scheme. Lines mark possible criteria to dissect the data with a chemical classification scheme in the ([Fe/H], [O/Fe]) plane. Lower panel: the locations in the ([Fe/H], [α/Fe]) plane of stars with spectroscopically determined chemical compositions from Bensby et al. (2005), Gilli et al. (2006) and Reddy, Lambert & Allende Prieto (2006).

$\sim$5 km s^{-1} (cf. Dehnen & Binney 1998). Hence, relative to the Sun, the asymmetric drift of the thin disc is $\sim$10 km s^{-1}.

Haywood (2008) showed that the population with moderate α enhancement is a superposition of stars that combine either lower metallicity (at fixed [α/Fe]) with fast rotation or higher metallicity with lower rotation. The former subgroup bears a clear outer-disc signature, while the latter subgroup associates with the thick disc by virtue of their slow rotation. Higher metallicities at given [α/Fe] point to a flatter trajectory in the ([α/Fe], [Fe/H]) plane of the relevant ISM, i.e. to faster metal-enrichment before SNeIa started to explode. Such fast enrichment is to be expected in the dense inner disc. Thus, the structure found by Haywood (2008) is an inevitable consequence of chemical evolution in the presence of radial mixing.

The middle panel of Fig. 9 shows that essentially all thick-disc stars are older than 6 Gyr. Most stars of the intermediate population are also this old, but whereas the modal age of the thick disc exceeds 10 Gyr, no stars in the intermediate population are older than 10 Gyr. The sharp rise in the number of thick-disc stars at $\sim$10 Gyr, just where the number of stars in the intermediate population plummets, is very striking. The purple curve in the central panel of Fig. 10 clarifies the cause of this feature by showing the age distribution of

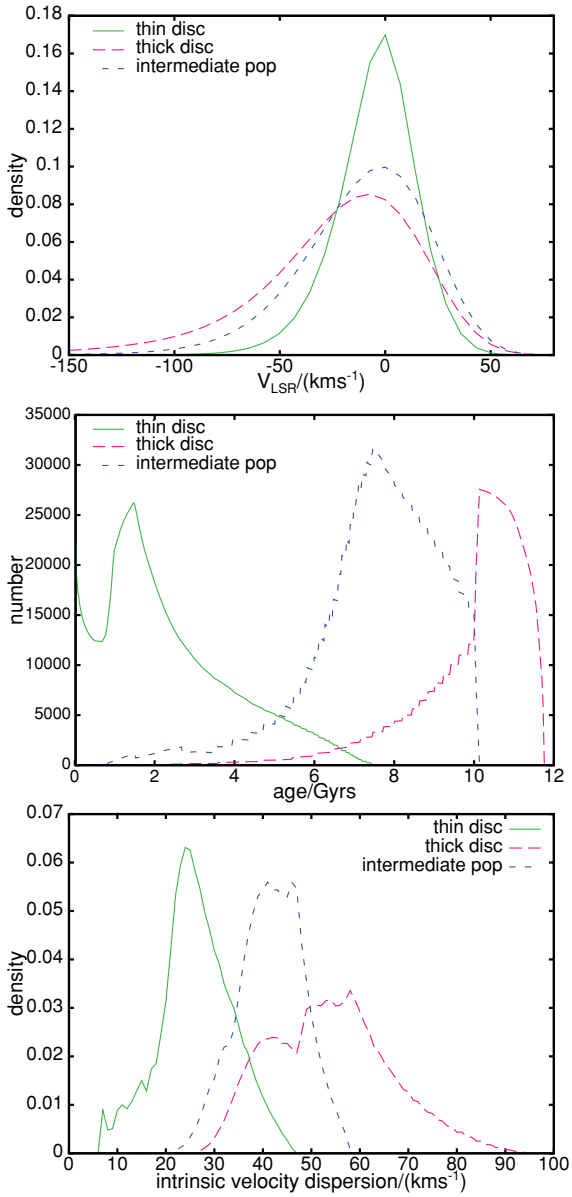

Figure 9. The top two panels show the distribution of stars from the three chemically selected populations in V velocity and age. The bottom diagram shows the distribution of stars by the velocity-dispersion parameter of the cohort to which they belong – see the description in text. The populations are the thin disc (green), the intermediate population (blue) and the thick disc (red). The curve showing the age distribution of the thin disc has been scaled down by a factor of 10 relative to the curves for the other two components. In the other panels, each curve is separately normalized to unity. The steps in the age distribution are artefacts arising from the model's radial resolution (0.25 kpc); a step is produced as an individual ring passes over the selection criterion.

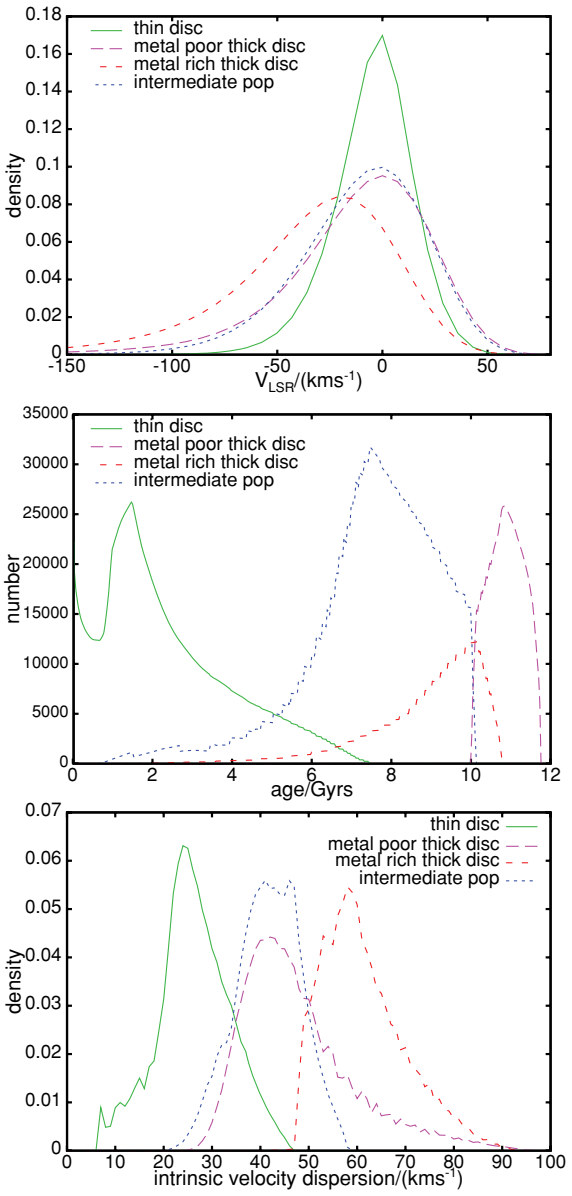

Figure 10. As Fig. 9 but with the thick-disc split into its metal-weak (purple) and metal-rich (red) parts, the latter being defined to comprise [Fe/H] > -0.8.

stars that have [O/Fe] > 0.56 (the horizontal boundary in Fig. 8) and [Fe/H] < -0.8. We see that all these metal-poor, highly α-enhanced stars are older than 10 Gyr, so the significance of a 10 Gyr age is that older stars formed before SNeIa started to enrich the ISM with iron. The purple curve in the top panel of Fig. 10 shows that the modal rotation velocity of these high-α stars is not far from circular. That is, the metal-poor thick disc has a smaller asymmetric drift than the portion of the thick disc that lies to the right of the division line in Fig. 8 (red curves in Fig. 10), which we henceforth refer to as the metal-rich thick disc because all its stars have [Fe/H] > -0.8. This metal-rich portion has an average asymmetric drift of $\sim$35 km s^{-1}, which is 30 km s^{-1} below the mean rotation velocity of the thin disc.

The green curve in the central panel of Fig. 9 shows that all thin-disc stars are younger than 7 Gyr and the rate of their formation appears to rise rapidly towards a peak at $\sim$1.5 Gyr. In reality, the SFR in the disc was monotonically declining throughout this period, so this apparent rise is entirely a selection effect. Several factors contribute to the detailed shape of the thin-disc age distribution in Fig. 9, including the restriction of the sample to a volume near the Galactic plane (which disfavours old stars) and the brightening of stars as they begin to turn-off the main sequence (which accounts for the peak at $\sim$1.5 Gyr).

The bottom panels of Figs 9 and 10 show decompositions of each population into isothermal cohorts. A decomposition is possible

because in the model each cohort of stars (stars formed at a given time and place) has a steadily increasing velocity dispersion. The plotted decompositions show the distribution of the current velocity dispersions for the cohorts that make up each population, weighted by the fractional contribution of the cohort to the population.

In Fig. 9, the isothermal decompositions of the thin disc (green) and intermediate population (blue) are similar except that the distribution for the intermediate population is shifted to the right by $\sim$20 km s^{-1}. The isothermal decomposition of the thick disc is bimodal. The purple curve in the bottom panel of Fig. 10 shows that the peak of this curve around 40 km s^{-1} is associated with the metal-poor thick disc. So, within our model the bulk of the metal-poor thick disc has smaller velocity dispersions than are found in the metal-rich thick disc. This chimes with the higher characteristic V velocities of the metal-poor thick disc in indicating that it is cooler and faster rotating than the metal-rich thick disc. The tail to high dispersions in the decomposition of the thick disc is contributed by a small number of very old stars that were formed at small radii, where the velocity dispersion is currently large.

By fitting the model's vertical density profile with the sum of two exponentials in $|z|$, SB09 concluded that in the model a fraction $f_{\rm thick} \sim 0.13$ of solar-neighbourhood stars belong to the thick disc; it followed that of the order of one-third of the entire disc mass is contributed by the thick disc. These numbers were in good agreement with the conclusions that Juric et al. (2008) and Ivezic et al. (2008) drew from SDSS counts of stars $\gtrsim$1 kpc from the plane. Using the present chemical decomposition into thin and thick discs, we find $f_{\rm thick} \sim 0.14$. In principle, this number does not have to agree with the value obtained from the density profile. It does agree well because at $|z| \gtrsim 1$ kpc the disc is dominated by stars that have thick-disc chemistry (Fig. 7).

Fig. 11 shows the vertical density profiles of the thin disc (green), thick disc (red) and the entire disc (blue). Fits of exponentials to the density profiles yield scaleheights of 268 pc for the thin disc and 822 pc for the thick disc. The two components of the latter have scaleheights 690 pc for the metal-poor thick disc and 890 pc for the metal-rich component. All components show more or less exponential profiles. The metal-poor thick disc has the strongest deviations from an exponential due to its being a mix of very old stars from

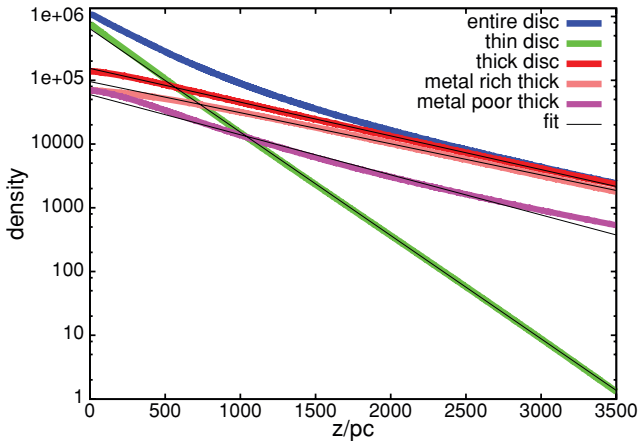

Figure 11. The vertical density profiles of the total disc (blue), thin disc (green), thick disc (red), the metal-poor thick-disc component (purple) and the metal-rich thick disc (orange). The thick-disc partition at $z = 0$ is 14 per cent, scaleheights of the single components are (measured between $z = 400$ and 3000 pc) $h_{\rm thin} = 270$ pc, $h_{\rm thick} = 820$ pc, $h_{\rm poor\,thick} = 690$ pc and $h_{\rm rich\,thick} = 890$ pc.

all over the disc with radically different intrinsic velocity dispersions. When a sum of exponentials is fitted to the measured vertical profile of the Galactic disc, good fits can be obtained with quite a wide range of scaleheights on account of a correlation between the scaleheights of the two discs and their normalizations. The fits above to our individual discs are within the range of observationally acceptable scaleheights (e.g. Juric et al. 2008), consistent with the thick disc identified by Juric et al. being close to what we have identified in the model using totally different criteria.

2.4 Inside–out formation?

For simplicity, the SB09 model does not accelerate the formation of the disc at small radii relative to large radii, as is required by the popular 'inside–out' model of disc formation. If the model were adjusted to include inside–out formation, the main change would be to the metal-poor thin disc, which would lose parts of its high-V wing. Hence, the inside–out scenario could be put in doubt by demonstrating that the V-distribution of the high-α stars extends significantly to $V > 0$, and that many high-V stars have ages in excess of 10 Gyr. Further, inside–out formation could give rise to some α enhanced, relatively metal-poor stars younger than $\sim$10 Gyr by the later onset of star formation in outer rings. Neither the thin disc nor the metal-rich thick disc would be strongly affected by the introduction of inside–out formation.

3 KINEMATIC DIVISION OF THE DISC

Because it is much easier to measure the velocity of a star than to determine its chemical composition (particularly its α-enhancement), nearly all analyses select stars kinematically. Our model provides an arena in which we can examine the extent to which kinematically selected samples of each component will be contaminated with stars from other components.

Samples of local stars such as those of Venn et al. (2004) and Bensby et al. (2005) are kinematically divided into thin- and thick-disc stars with the aid of model distribution functions (DFs) for each component: as described in Bensby et al. (2003), each star is assigned to the component whose DF is largest at the star's velocity. Both DFs are of the type introduced by Schwarzschild (1907), namely

$$f(U, V, W) = k f_i \exp\left[-\frac{U^2}{2\sigma_U^2} - \frac{(V - V_{\rm asym})^2}{2\sigma_V^2} - \frac{W^2}{2\sigma_W^2}\right], \qquad (2)$$

where all components are with respect to the LSR, $k = (2\pi)^{-3/2} (\sigma_U \sigma_V \sigma_W)^{-1}$ is the standard normalization constant, f_i is the relative weight of the population. The dispersions σ_i assumed for the thick disc are larger than those assumed for the thin disc, so high-velocity stars tend to be assigned to the thick disc. Because $V_{\rm asym}$ is assumed to be $\sim$30 km s^{-1} larger for the thick disc than the thin, stars with lagging rotation velocities and therefore guiding centres at $R < R_0$ also tend to be assigned to the thick disc. This effect is reinforced by the fact that the dispersions must increase inwards, so stars with guiding centres well inside R_0 are also likely to be high-velocity stars. Consequently, the 'thick-disc' stars in Venn et al. (2004) and Bensby et al. (2005) tend to belong to the inner disc. In the context of our model, this fact explains why Bensby et al. (2003) found a long tail of 'thick-disc' stars that have higher [Fe/H] at a given [α/Fe] than the 'thin-disc' stars.

We examine the effectiveness of kinematic selection in two ways. First, in each panel of Fig. 12, we plot the distribution in a Toomre

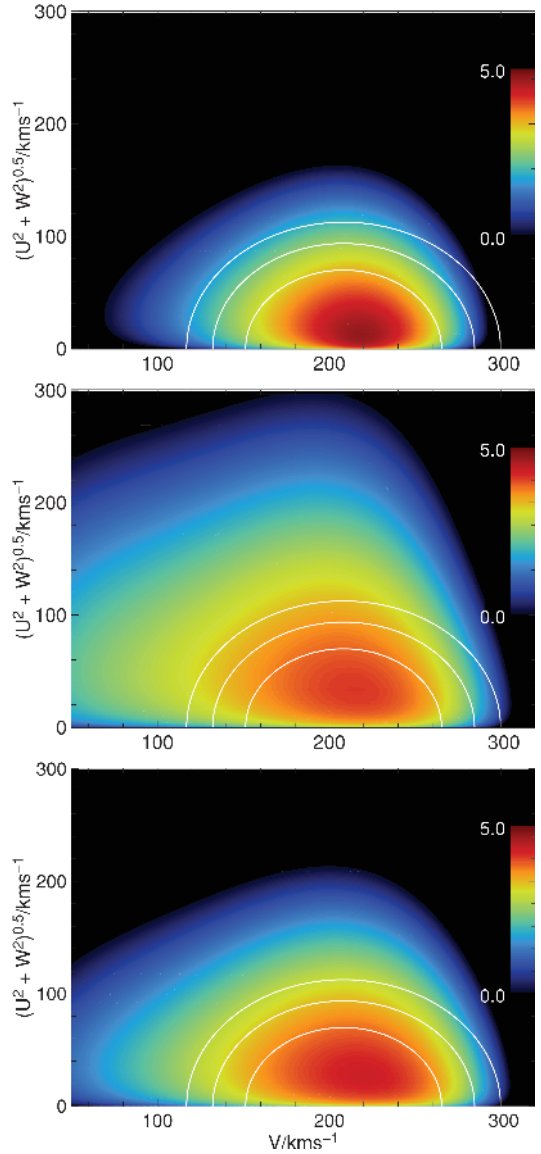

Figure 12. From top to bottom panels, Toomre diagrams for the chemically selected thin-disc, thick-disc and intermediate populations within the model's solar neighbourhood. Colour encodes the density of stars and ranges over five orders of magnitude. Shown in white are curves on which the probability of star belonging to the thick disc by the criteria of Bensby et al. (2003) is constant given $W = 0.55U$; on these curves from inwards out the thick-disc probability is 0.1, 1.0 and 10.0 times the thin probability. Inside the inner curve, stars were deemed to belong to the thin disc, and outside the outer curve they were assigned to the thick disc.

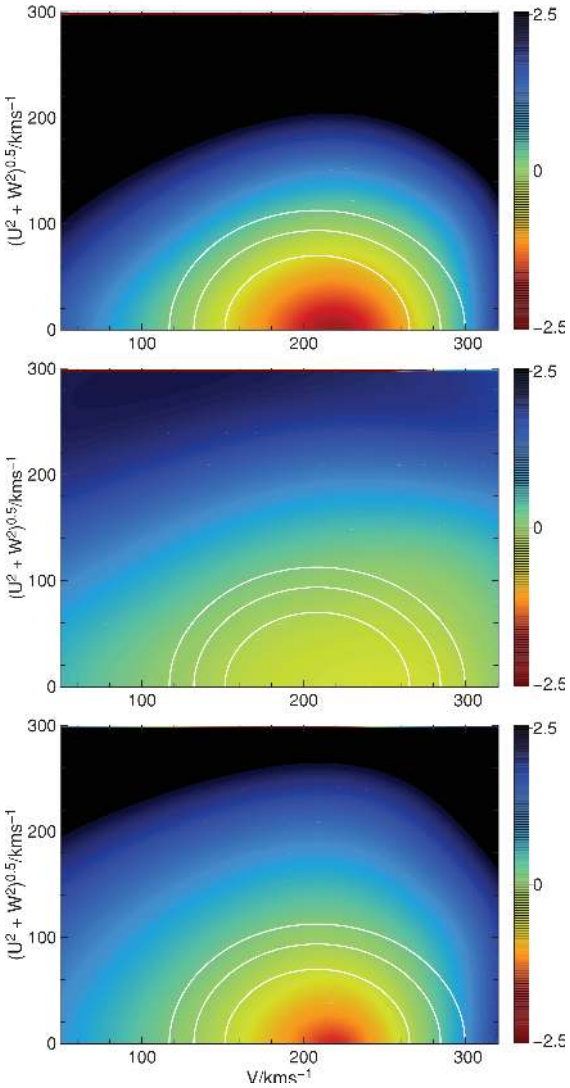

Figure 13. From top to bottom panels, the ratio of thick by thin disc, thick disc by intermediate disc and intermediate disc by thin-disc stars at each point in the Toomre diagram when metal-poor and metal-rich thick disc are combined. Colours show the log of the ratio with values in the range (−2.5, 2.5). White contours are the same as in Fig. 12.

diagram of each of the components that we have identified chemically. Subsequently, in Figs 14–16 we examine the distributions in the ([α/Fe], [Fe/H]) plane of model stars that have been kinematically identified as belonging to the thin or thick disc.

Fig. 12 shows the Toomre diagrams for the thin, thick and intermediate components, respectively. In Fig. 12, all densities are separately normalized to unity, while Fig. 13 shows the density ratios of components in the Toomre diagram. The extensive overlap of the chemically selected populations in the Toomre diagram is striking, but a natural consequence of the approximately Gaussian nature of the DFs of each component, which implies that the density of thick-disc stars peaks at velocities close to the LSR, which is where the thin disc is dominant. Consequently, no kinematic selection of stars from a particular chemical component can be very clean. This point is underlined by the white curves in Figs 12 and 13, which are such that Bensby et al. (2003) classified stars with[1] $W = 0.55U$ as thick disc if they lay outside the outermost white curve and thin disc if they lay inside the innermost curve. The top panel in Fig. 12 shows that this criterion does exclude most thin-disc stars from a thick-disc sample. However, the upper two panels of Fig. 13 imply substantial contamination of the thick disc: in these panels, red indicates a region where most stars are not thick-disc stars, yet at lower right red extends significantly beyond the outermost white curve in both panels. From Fig. 12, it is evident that a slightly cleaner kinematic separation could be obtained if a non-Gaussian DF were

[1] For general values of W/U, the Bensby et al. (2003) kinematic selection criterion, which is three-dimensional, cannot be plotted in a Toomre diagram because the latter is two-dimensional. Hence, we choose the approximate ratio of the dispersion components for our graphs.

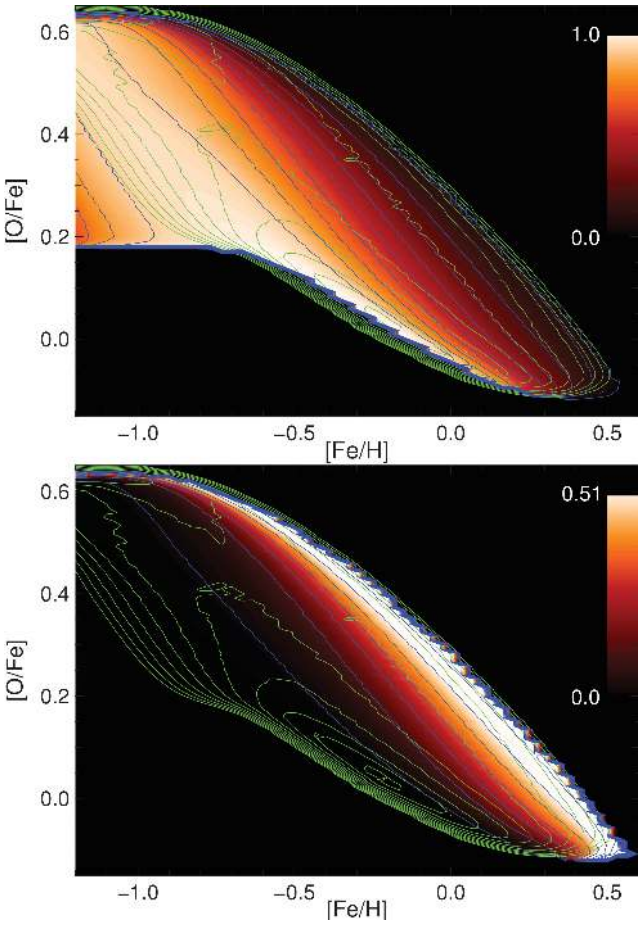

Figure 14. Selection probabilities using the kinematic selection function of equation (2) for the thin (upper panel) and thick disc (lower panel). Blue contours give lines of same selection probability for a star at a certain chemical composition with levels running from 0.01 to 0.91 with a 0.1 spacing for the thin disc and from 0.01 to 0.61 with a 0.05 spacing for the thick disc. Colours encode the selection probability and the green contours show lines of the model's entire disc population density at a 0.5 dex spacing.

used in place of (2), but the main problem with kinematic selection is the extensive overlap of the components in velocity space.

From the centre panel of Fig. 12, we see that a large fraction of the thick disc is also excluded from a kinematically selected sample of thick-disc stars, and many of the excluded stars will be assigned to the thin disc because they lie within the region reserved for the thin disc.

Fig. 14 shows the probabilities used by Bensby et al. (2003) for a star to be assigned to the thin (upper panel) and thick (lower panel) discs. The probability of being assigned to the thin disc is large in a broad swath that runs from [O/Fe] = 0.6 and [Fe/H] = −1.2 down to the lower edge of the populated region of the diagram, and then on to solar [Fe/H] and above. Thus, the kinematically selected thin disc includes high-α stars in contrast to our chemically selected thin disc. Kinematic selection does not confine the thin disc to stars near the ridgeline of the chemical thin disc because the low-velocity dispersions and high rotation velocities characteristic of large radii cause most stars formed at large radii to be kinematically assigned to the thin disc. Stars in the more metal-rich flank of the chemical thin-disc ridge tend to be assigned partly to the intermediate population, or even (for the highest metallicities/innermost rings of origin) to the thick disc.

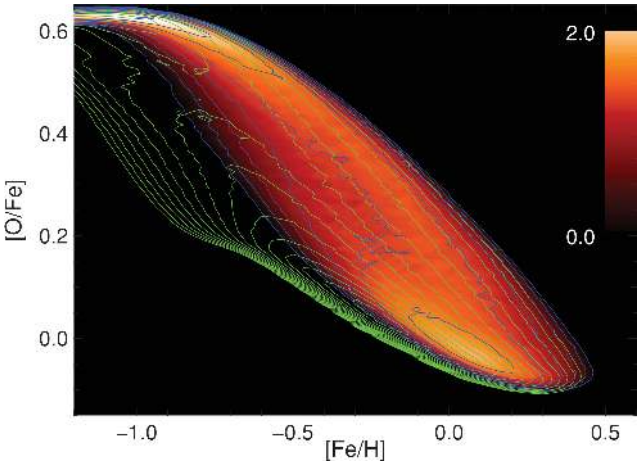

Figure 15. Green lines show the density contours in the ([Fe/H], [O/Fe]) plane of the entire disc population with a 0.3 dex spacing. Colours and blue contours show the absolute density of stars selected kinematically according to equation (2) to the thick disc with 0.3 dex contour spacing.

In Fig. 14, the probability of a star being assigned to the thick disc is high along the sloping upper edge of the populated region of the ([Fe/H], [α/Fe]) plane. Consequently, the Bensby et al. (2003) kinematic criterion for being a member of the thick disc does pick stars that belong to the thick disc by our chemical definition. However, the density of stars actually assigned to the thick disc by the kinematic criterion, which is shown in Fig. 15, extends below the sloping dashed line in Fig. 8 because the density of stars assigned to the thick disc is the product of the assignment probability plotted in Fig. 14 and the density of stars in the ([Fe/H], [α/Fe]) plane, which declines steeply as the edge of the populated region is approached. In fact, the ridge of kinematically selected thick-disc stars leaves the upper edge of the populated region at the α-enhancement turn-off and then runs downwards parallel to the thin-disc ridge at an offset of $\simeq$0.3 dex in [Fe/H], just as reported by Bensby et al. (2003) and Venn et al. (2004). Moreover, the zone of thick-disc stars merges with the thin-disc population at [Fe/H] $\simeq$ 0, which was one of the main findings of Bensby et al. (2003).

The upper panel of Fig. 16 shows the age distributions of the kinematically selected components, and should be compared with the middle panel of Fig. 9. When kinematically selected, the thin disc has a long tail of very old stars. Conversely, the age distributions of the thick disc and especially the intermediate population extend to much younger ages when these components are kinematically selected. It is inevitable that a kinematically selected thin disc will contain old stars that properly belong to either the thick disc or the intermediate population because stars with small velocities relative to the LSR must be assigned to the thin disc, yet any plausible DF for the thick disc will be significantly non-zero at such velocities. The assignment of young stars to the intermediate population reflects the red colour in the lower-right corner of the centre panel of Fig. 13 that was discussed above.

The lower panel of Fig. 16 shows histograms of the ages of GCS stars in Haywood (2008) when stars are assigned to components using the kinematic criteria of Bensby et al. (2003) – the corresponding histograms of the ages given by Holmberg et al. (2007) is very similar. Clearly, the histograms are badly distorted by errors in the ages, which scatter stars to unrealistically large ages, so the horizontal scale of the lower panel is nearly twice that of the upper

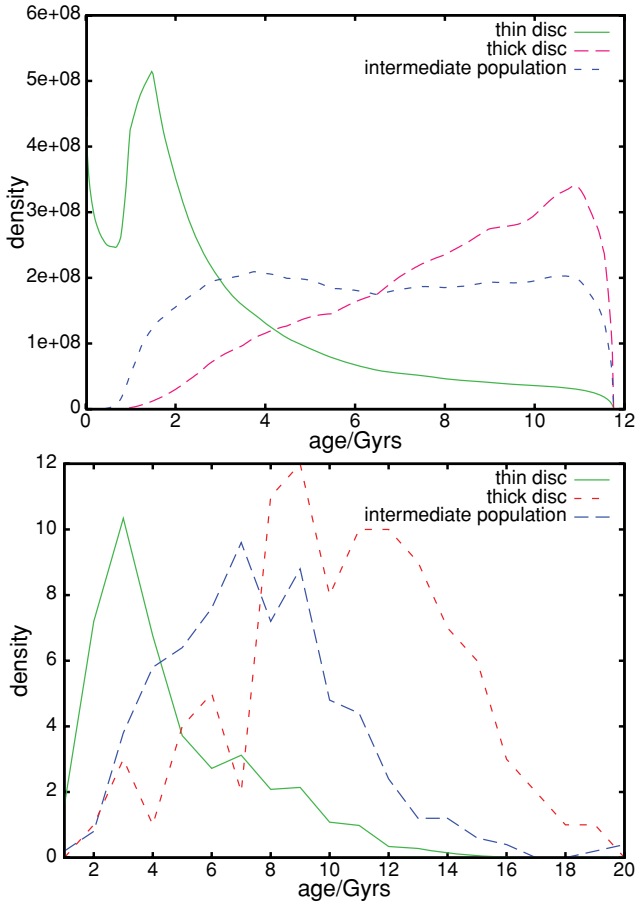

Figure 16. Upper panel: model age distributions for the three kinematically selected components in the model. As in Figs 9 and 10, the curve for thin disc has been lowered by a factor of 50 and that for the intermediate population by a factor 5 relative to the curve for the thick disc. Lower panel: the distribution of measured ages of GCS stars given by Haywood (2008) with stars kinematically assigned to components using the Bensby et al. (2003) criteria. Stars with age younger than 0.5 Gyr are not taken into consideration due to high errors. When the ages published by Holmberg et al. (2007) are used, the lower panel does not change significantly.

panel. None the less, the lower panel seems to be as consistent with the upper panel as the large errors permit.

The numbers of model stars in the solar neighbourhood that are kinematically assigned to the three components analysed in the upper panel of Fig. 16 is thin : intermediate : thick = 1 : 0.099 : 0.0239. The same ratios for the observational sample analysed in the lower panel of Fig. 16 are 1 : 0.085 : 0.029 in satisfactory agreement with the model's prediction, but the agreement is actually better than this comparison suggests, when one accounts for the difference between the selection functions used to select the observed stars in the lower panel of Fig. 16. If we use the GCS sample without binaries, which our selection function was designed for, the ratios are changed to 1 : 0.095 : 0.029. When we further remove likely halo stars, the observational thick-disc fraction shrinks to ∼0.025. Indeed, the fraction of the local column of thick-disc stars that resides near the Sun is sensitive to the distribution of W velocities. The latter is not tightly constrained because one of the least satisfactory aspects of the model is the absence of dynamical coupling between horizontal and vertical motions, which obliges one to make an arbitrary assumption about the variation with random velocity in the shape of the velocity ellipsoid. It is worth noting that the model probably has more metal-rich stars high above the Sun than it should have as a consequence of our assumption that high-velocity stars are as susceptible to churning as low-velocity stars.

4 CONCLUSIONS

The thick disc is the Proteus of Galactic physics: depending on which questions you ask it changes its shape. Although it has been identified by both its extended vertical density profile and its distinct kinematics, it is most usefully characterized chemically, not least because chemical composition is a permanent feature of a star, whereas distance from the plane and peculiar velocity are ever-changing properties. Moreover, chemical composition is intimately connected to the time and place of the star's birth.

The determination of the chemical composition of large numbers of old main-sequence stars is feasible only for samples of nearby stars. Unfortunately, the nearby stars constitute a strongly biased sample of the whole Galactic disc. It is absolutely essential to interpret the statistics of the solar neighbourhood in the context of these biases. We have used our model Galaxy to explore these biases, and in particular the relationship between the components one obtains by assigning stars to them on the basis of their kinematics or their chemistry. A very straightforward conclusion is that kinematic selection inevitably misallocates many stars, adding both old stars to the thin disc and young stars to the thick disc.

We have shown that our model provides a consistent interpretation of observations of the solar neighbourhood in which components are identified as regions of the ([Fe/H], [α/Fe]) plane. Thin-disc stars lie in a narrow ridge of high density between [Fe/H] ∼ −0.65 and 0.15 that forms part of the lower edge of the populated part of the ([Fe/H], [α/Fe]) plane. The metal-rich thick disc occupies a broader swath of the ([Fe/H], [α/Fe]) plane that runs parallel to the downward-sloping ridge of the thin disc and ∼0.3 in [O/Fe] higher. The metal-rich thick disc extends in [Fe/H] from ∼ −0.9 to well above 0, where it merges with the thin disc. At its low-metallicity high-α end, the metal-rich thick disc touches the metal-poor thick disc, in which [O/Fe] $\simeq 0.63 \pm 0.5$ and [Fe/H] goes at least down to ∼ −1.4. There is an 'intermediate population' of stars that in the ([Fe/H], [α/Fe]) plane lie between the thin and thick discs, but the density of such stars in the ([Fe/H], [α/Fe]) plane is relatively low. Thus, the two discs are well-defined structures.

Thin-disc stars are all younger than 7 Gyr and are on fairly circular orbits. Their values of [Fe/H] and rotation velocity V are correlated in the sense that higher V implies lower [Fe/H]. The stars of the metal-rich thick disc are nearly all older than 8 Gyr. Most are on significantly non-circular orbits with guiding centres inside R_0, and a significant number have $V < -100$ km s^{-1}. Specifically, the metal-rich thick disc can be considered to be a superposition of isothermal components with radial velocity dispersions between 50 and 80 km s^{-1}, strongly peaked around 60 km s^{-1}. The metal-poor thick disc consists exclusively of stars older than 10 Gyr. Its stars have on average more angular momentum and smaller velocity dispersions than the stars of the metal-rich thick disc. Among the population of strongly α-enhanced stars, there is (cf. Fig. 4) an extremely strong negative correlation between α and V.

Meléndez et al. (2008) remarked that the thick disc has similar properties to the Galactic bulge. This conclusion is natural in the context of our model, in which the metal-rich thick disc is made up of stars that have migrated to the Sun from the inner disc, where rapid early star formation enriched the ISM to significant metallicities before SNeIa began to lower [α/Fe]. It is to be expected that many

of the stars that formed alongside the thick-disc stars of the solar neighbourhood are now bulge stars.

Perhaps the most uncertain aspect of the modelling is our assumption that a star's probability of being 'churned' to a different angular momentum is independent of the star's random velocity. Since Sellwood & Binney (2002) did not investigate the dependence of churning probability on random velocity, our assumption could be significantly in error, and it is not implausible that stars with large random velocities have low churning probabilities. In this case, the thick disc would be less radially mixed than our model predicts. We will shortly investigate the dependence of churning probability on random velocity.

Given our model's success in synthesizing studies of the Galactic disc into a coherent picture, it is useful as it stands regardless of the theoretical considerations that motivated its construction. However, it was not made by searching an extensive parameter space for a model that would fit the studies described here. Rather it was made by building a code that combined standard chemical evolution modelling with a model of dynamical evolution that reflects the understanding of how spiral structure works that Sellwood & Binney (2002) gained from *N*-body models and analytical dynamics. Its two free parameters were determined from the model's fit to the metallicity gradient in the ISM and to the metallicity distribution of the GCS stars given in Nordström et al. (2004) and Holmberg et al. (2007). Hence, we consider the model's ability to reproduce the data sets of Fuhrmann (1998), Bensby et al. (2003, 2005), Venn et al. (2004), Reddy et al. (2006), Haywood (2008), Juric et al. (2008) and Ivezic et al. (2008) is remarkable and suggests that it has a sound physical basis.

The key respect in which the model goes beyond traditional models of chemical evolution is its inclusion of radial migration by stars and inward flow by gas. Inward flow of gas is important for the model's success because it establishes a much steeper metallicity gradient than traditional models produce. The radial migration of stars is absolutely key, because it structures the thick disc. Moreover, it explains the significant spread in [Fe/H] within the local thin disc, and the correlation that Haywood (2008) identified between [Fe/H] and V.

The discovery that the thick disc overlaps the thin disc in [Fe/H] presented a challenge to conventional models of chemical evolution because it implies that there are thick-disc stars that have both [α/Fe] and [Fe/H] higher than in some thin-disc stars. The lower values of [α/Fe] in the thin-disc stars imply earlier times of birth, so how come [Fe/H] is lower? The conventional response to this challenge is to suppose that some violent event led to a suspension of star formation in the disc, and that during this hiatus a massive injection of metal-poor gas lowered [Fe/H] in the ISM (Chiappini, Matteucci & Gratton 1997; Chiappini, Matteucci & Romano 2001). An objection to this scenario is that many other galaxies have thick discs with similar properties to ours (Yoachim & Dalcanton 2006), so thick-disc formation should not require special circumstances. We do not press this argument but would strongly make the point that a model of chemical evolution that includes only *essential* physics and has a single, early, maximum in the SFR and a monotonically rising value of [Fe/H] at each radius automatically produces a thick disc with just the properties observed locally. In fact, an α-enhanced thick disc forms because the speed at which [Fe/H] rises declines as one moves outwards, so the value attained by [Fe/H] when SNeIa start to lower [α/Fe] increases inwards. Spiral structure and the Galactic bar scatter α-enhanced stars formed at small radii on to more eccentric and more inclined orbits and even scatter some of them on to orbits of sufficiently high angular momentum that they are found in the solar neighbourhood. Readers who want to believe in a violent origin of the thick disc may continue to do so. But, they should be aware that the simplest model of the chemodynamical evolution of the disc that includes all relevant physics reproduces the data. Hence, there is absolutely no *evidence* that the thick disc has a violent origin.

ACKNOWLEDGMENTS

RS acknowledges financial and material support from Max-Planck-Gesellschaft, Stiftung Maximilianeum and Studienstiftung des Deutschen Volkes.

REFERENCES

Aumer M., Binney J., 2009, MNRAS, 397, 1286
Bensby T., Feltzing S., Lundström I., 2003, A&A, 410, 527
Bensby T., Feltzing S., Lundström I., Ilyin I., 2005, A&A, 433, 185
Chiappini C., Matteucci F., Gratton R., 1997, ApJ, 477, 765
Chiappini C., Matteucci F., Romano D., 2001, ApJ, 554, 1044
Colavitti E., Matteucci F., Murante G., 2008, A&A, 483, 401
Dehnen W., Binney J., 1998, MNRAS, 298, 387
Förster F., Wolf C. Podsiadlowski Ph., Han Z., 2006, MNRAS, 368, 1893
Fuhrmann K., 1998, A&A, 338, 161
Gilli G., Israelian G., Ecuvillon A., Santos N. C., Mayor M., 2006, A&A, 449, 723
Gilmore G., Reid N., 1983, MNRAS, 202, 1025
Haywood M., 2008, MNRAS, 388, 1175
Holmberg J., Nordström B., Andersen J., 2007, A&A, 475, 519
Ivezic Z. et al., 2008, ApJ, 684, 287
Jenkins A., 1992, MNRAS, 257, 620
Juric M. et al., 2008, ApJ, 673, 864
Just A., Jahreiss H., 2007, preprint (arXiv0706.3850)
Kennicutt R. C., 1998, ApJ, 498, 541
Lewis J. R., Freeman K. C., 1989, AJ, 97, L139
Mannucci F., Della Valle M., Panagia N., 2006, MNRAS, 370, 773
Meléndez J. et al., 2008, A&A, 484, L21
Nordström B. et al., 2004, A&A, 418, 989
Reddy B. E., Lambert D. L., Allende Prieto C., 2006, MNRAS, 367, 1329
Roskar R., Debattista V. P., Stinson G. S., Quinn T. R., Kaufmann T., Wadsley J., 2008, 675, L65
Schönrich R., Binney J., 2009, MNRAS, 396, 203 (SB09)
Schwarzschild K., 1907, Göttingen Nachr., 614
Sellwood J. A., Binney J., 2002, MNRAS, 336, 785
Venn K. A., Irwin M., Shetrone M. D., Tout C. A., Hill V., Tolstoy E., 2004, AJ, 128, 1177
Yoachim P., Dalcanton J. J., 2006, AJ, 131, 226

This paper has been typeset from a TEX/LATEX file prepared by the author.